Journal of Solid State Chemistry 183 (2010) 2636–2643

Contents lists available at ScienceDirect

Journal of Solid State Chemistry

journal homepage: www.elsevier.com/locate/jssc

Pressure-induced structural transformations in lanthanide titanates: La_2TiO_5 and Nd_2TiO_5

F.X. Zhang *, J.W. Wang, M. Lang, J.M. Zhang, R.C. Ewing *

Department of Geological Sciences, The University of Michigan, Ann Arbor, MI 48109, USA

ARTICLE INFO

Article history:
Received 18 May 2010
Received in revised form
1 September 2010
Accepted 12 September 2010
Available online 17 September 2010

Keywords:
RE_2TiO_5
Superstructure
Pressure
Phase transition

ABSTRACT

The structure of orthorhombic rare earth titanates of La_2TiO_5 and Nd_2TiO_5, where Ti cations are in five-fold coordination with oxygen, has been studied at high pressures by X-ray diffraction (XRD), Raman scattering measurements, and quantum mechanical calculations. Both XRD and Raman results indicated two pressure-induced phase transitions during the process. An orthorhombic super cell ($a \times b \times 2c$) formed at a pressure between 6 and 10 GPa, and then transformed to a hexagonal high-pressure phase accompanied by partial decomposition. The hexagonal high-pressure phase is quenchable. Detailed structural analysis indicated that the five-coordinated TiO_5 polyhedra remain during the formation of super cell, but the orthorhombic-to-hexagonal phase transition at high pressures is a reconstructive process, and the five-fold Ti–O coordination increased to more than 6. This phase transition sequence was verified by quantum mechanical calculations.

1. Introduction

Rare earth titanates have received considerable attentions in recent years due to the lanthanide perovskites, $LnTiO_3$ and pyrochlore-related structures, which show interesting structural properties, physical properties, and broad applications in engineering [1–10]. In all of these compounds, Ti is in six-fold coordination with oxygen, forming a corner-sharing octahedral framework, and the larger lanthanide elements occupy the voids in the framework. The La–Ti–O ternary system is more complicated, as $La_2Ti_2O_7$ does not have the pyrochlore structure, but forms a perovskite-related phase, and there are many homologous polymorphs with different compositions in this ternary system [11]. Their structures are comparable to the simplest $LaTiO_3$ perovskite. However, there is a different structure-type, which was discovered in this ternary system several decades ago [12]. The phase is orthorhombic with composition of La_2TiO_5, where Ti is five-coordinated with oxygen forming an off center square pyramid. Neighbor polyhedra are corner-shared and form in a chain along the *c*-axis (Fig. 1). The larger La^{3+} has 7 nearest-neighbor oxygens, which is lower than the coordination number in any of the other ternary compounds in this system. Though this kind of geometry is not often seen in nature, all the light lanthanide titanates with composition of Ln_2TiO_5 and *Ln* elements from La to Dy (including Y), form this orthorhombic structure. In addition, RE_2TiO_5 with medium-sized lanthanides have different structures at high temperatures, such as that a hexagonal phase was confirmed for Ln_2TiO_5, where *Ln* = Gd, Tb, Dy, Ho, and Y, at temperature higher than 1300 °C [13,14]. All of the heavy lanthanides with ionic radius less than Ho, Ln_2TiO_5 have a cubic structure, which is isostructural with the cubic pyrochlore $Ln_2Ti_2O_7$, but some cation antisite defects are included [8,9]. For La_2TiO_5, the orthorhombic structure is stable up to melting at temperature above 1700 °C [13]. Although there are some recent studies on the phase relations for these structures [13–15], the properties of these oxides are not well known.

Many high pressure studies have been completed on the six-coordinated perovskite structure [16–19]. The six-coordinated TiO_6 is quite stable in perovskite, and high pressures can be used to "tune" its orientation, which affects their physical properties [20]. In pyrochlore, due to the structural disordering, the TiO_6 octahedron is not stable, and the structure becomes amorphous at high pressures [21,22]. Because the five-coordinated TiO_5 is not often seen in oxides, the structural stability of RE_2TiO_5 at high pressure is thus interesting. In these experiments, two pressure-induced phase transitions were clearly evident in the X-ray diffraction and Raman scattering measurements. First principle calculations of the lattice energetic of these phases were consistent with the experimental results. Our experiments revealed that the isostructural oxide Nd_2TiO_5 has similar structural behavior to that of La_2TiO_5 at high pressures.

2. Experimental details

Samples of La_2TiO_5 and Nd_2TiO_5 were synthesized by solid-state reaction from the corresponding oxides of La_2O_3 (99.9%), Nd_2O_3 (99.9%), and TiO_2 (99.9%). Well-mixed powders were

* Corresponding authors.
E-mail addresses: zhangfx@umich.edu, zfx6506@yahoo.com (F.X. Zhang), rodewing@umich.edu (R.C. Ewing).

0022-4596/$ - see front matter © 2010 Elsevier Inc. All rights reserved.
doi:10.1016/j.jssc.2010.09.014

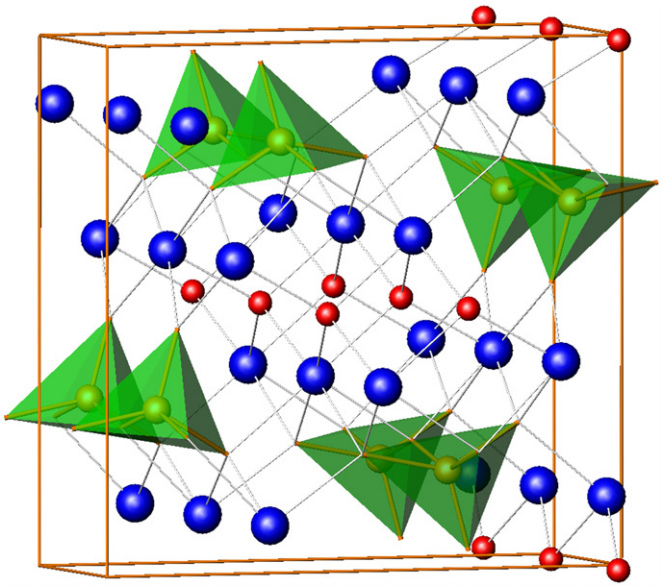

Fig. 1. Schematic crystal structure of orthorhombic Ln_2TiO_5 with space group *Pnam*. The polyhedron is TiO_5, which is Ti centered and five-coordinated with oxygen. Lanthanide elements are seven coordinated with oxygen.

pressed into pellets and first fired at 1200 °C for 1 day. In order to make the reaction homogeneous, the pellets were reground and reshaped and heated at 1450 °C for 2–3 days. The structure of the samples was identified by powder X-ray diffraction. Typically, the grain size of the synthetic powders was in 1–10 μm based on TEM observations. There is no size effect to this kind of ceramics when the grain size is in micrometers scale [23]. For the high-pressure experiments, a symmetric diamond anvil cell with a pair of 300 μm culet diamond anvils was used. A hardened stainless steel gasket was indented to a thickness of ~40 μm, and a hole of 100–120 μm was drilled in the center as the pressure chamber. Methanol/ethanol (4/1) liquid served as the pressure-transmitting medium. The *in situ* X-ray diffraction experiments were mainly performed at National Synchrotron Light Source, Brookhaven National Laboratory with monochromatic X-ray beam (30.5 KeV and size 25 × 30 μm^2). In order to solve the crystal structure of the high-pressure phases, some high quality XRD patterns were collected at 16-ID-B of HPCAT, Advanced Photon Sources with wavelength of 0.3681 Å. All of the Debye images at both beam stations were collected with CCD detectors and then integrated into one dimensional XRD patterns with software Fit2D [24]. Pressure in all of the experiments was measured by the standard ruby fluorescence method. High pressure Raman spectra were measured with a liquid-nitrogen cooled CCD and activated with green light of an Ar laser (514.31 nm). The lattice parameters were derived from Rietveld refinement of the observed XRD patterns with program Fullprof in the platform of Winplotr [25]. The lattice parameters were indexed from the individual peaks with Dicvol [26], and the space group was selected based on extinction rules. The structure of the superlattice formed in La_2TiO_5 above 5 GPa was solved directly using EXPO2009 [27]. The second high pressure phase was found to have a structure closely related to that of Na_2SO_4.

Quantum mechanical calculations were performed using the Density Functional Theory (DFT) framework, and plane wave basis sets as implemented in the VASP package [28]. The Projector-Augmented Wave method (PAW) [29] and exchange-correlation as parameterized by the Perdew–Wang 91 (PW91) functional [30,31] were applied in the Generalized Gradient Approximation (GGA-PAW) [32]. The total energy and volume calculations for the two systems were completed by optimizing the structures without symmetry constraints. The Monkhorst–Pack scheme for integration in the Brillouin zone was adopted. Test runs were performed to test the energy convergence on the *k*-point grid and energy cutoff. A 5 × 5 × 5 *k*-point grid was used for the monoclinic and tetragonal phases, and a 7 × 7 × 4 *k*-point grid was used for the high-pressure tetragonal phase. The energy cutoff for the plane-wave basis set is 520.00 eV (38.22 Ry) for all calculations. These parameters settings were sufficient for energy convergence.

3. Results and discussions

3.1. Superlattice formation

The synthetic powders of La_2TiO_5 and Nd_2TiO_5 are orthorhombic, and the measured XRD patterns with X-ray wavelength λ=0.486 Å were well refined with space group of *Pnam* (Fig. 2). There are two La, one Ti, and five independent O atoms in the unit cell, and all atoms occupy the 4*c* positions. The detailed lattice parameters, atomic coordinates and fitting results are listed in Table 1. The structural parameters of La_2TiO_5 and Nd_2TiO_5 are in good agreement with those of Gd_2TiO_5 in Ref. [13].

A small amount of the powders were loaded in a diamond anvil cell together with methanol/ethanol mixture as the pressure-transmitting medium. The selected XRD patterns at various pressures are shown in Fig. 3. Approximately at 10 GPa, the XRD pattern clearly indicated that there is a pressure-induced phase transition in both samples. The number of diffraction peaks of the high-pressure phases is much less than those of the orthorhombic structure, which suggested a higher symmetry structure for the high-pressure phase. By careful checking of the XRD patterns below 10 GPa, we found that there is another new phase formed before the phase transition at 10 GPa in both samples. Fig. 4 shows the XRD patterns of La_2TiO_5 and Nd_2TiO_5 at pressure below 10 GPa. There are some new peaks in the XRD patterns at pressures above 5.1 and 7.9 GPa in the samples of La_2TiO_5 and Nd_2TiO_5, respectively. However, the mainly character of the XRD patterns shows no major changes before and after the appearance of these new peaks. This suggests that the new phase has a close relationship to the initial orthorhombic structure. By indexing the XRD patterns, we found that the new peaks cannot be generated by decreasing the symmetry, but with the original lattice parameters. However, all of the diffraction peaks can be well indexed if the lattice parameters are expanded. The indexed patterns indicated that all of the diffraction peaks can be indexed with a super orthorhombic unit cell, $a \times b \times 2c$, where, *a*, *b*, and *c* are the lattice parameters of the starting orthorhombic phase. Thus the orthorhombic La_2TiO_5 and Nd_2TiO_5 form a superlattice at pressures between 5 and 10 GPa before the second high-pressure phase transition occurs.

The experimental results revealed that the formation of superlattice at lower pressure is common to all other 215 phases of RE_2TiO_5 (*RE*=Sm, Eu, Gd, Dy, and Y). The indexing of more than 50 individual peaks showed that the diffraction maxima obey the following restrictions: $h=2n$ for $h\,0\,0$ and $k=2n$ for $0\,k\,0$ (*n* are integers). The extinction rules indicated that possible space groups for the super cell are *Pma*2 (28), *Pmam* (51), and $P2_1am$ (26). We tried to solve the crystal structure by the direct method from the observed diffraction patterns with all the three possible space groups, and a reasonable structure model can only be obtained with space group of $P2_1am$. Using direct structure solution software EXPO on the XRD pattern of La_2TiO_5 at 7.5 GPa, which was collected at APS, 9 heavy and 11 light atomic positions were generated based on the electron density map of the unit cell. The 9 heavy sites were assigned as 6 La and 3 Ti atoms, and all the

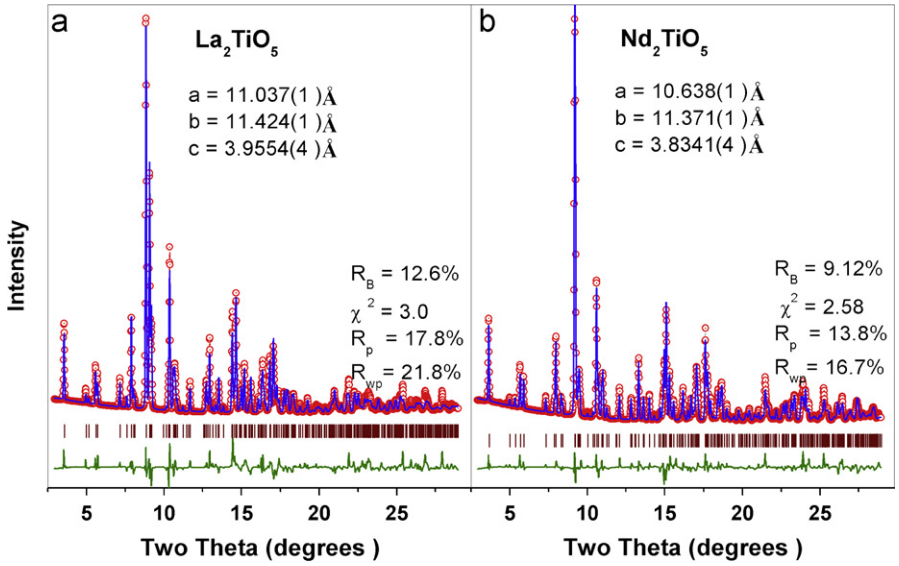

Fig. 2. Rietveld refinement results of the XRD patterns of La_2TiO_5 and Nd_2TiO_5 at ambient conditions (λ=0.486 Å).

Table 1

The refined atomic coordinates of orthorhombic La_2TiO_5 and Nd_2TiO_5 in space group of *Pnam*. The lattice parameters are a=11.0373(11) Å, b=11.4245(11) Å, c=3.9554(4) Å, R_B=12.6%, and χ^2=3 for La_2TiO_5 and a=10.6382(11) Å, b=11.3705(11) Å, c=3.8341(4) Å, R_B=9.1%, and χ^2=2.58 for Nd_2TiO_5.

Atom	Wyckoff	x/a	y/b	z/c	Atom	x/a	y/b	z/c
La1	4c	0.1355(4)	0.0615(3)	1/4	Nd1	0.1369(4)	0.0579(3)	1/4
La2	4c	0.4040(4)	0.2148(4)	3/4	Nd2	0.3934(3)	0.2188(3)	3/4
Ti	4c	0.1897(9)	0.3713(12)	1/4	Ti	0.1813(9)	0.3764(12)	1/4
O1	4c	−0.002(3)	0.105(3)	3/4	O1	0.022(3)	0.109(4)	3/4
O2	4c	0.263(3)	0.036(4)	3/4	O2	0.268(4)	0.027(3)	3/4
O3	4c	0.234(3)	0.373(4)	3/4	O3	0.232(3)	0.364(4)	3/4
O4	4c	0.259(3)	0.193(3)	1/4	O4	0.274(4)	0.203(4)	1/4
O5	4c	0.041(3)	0.341(3)	1/4	O5	0.003(4)	0.335(3)	1/4

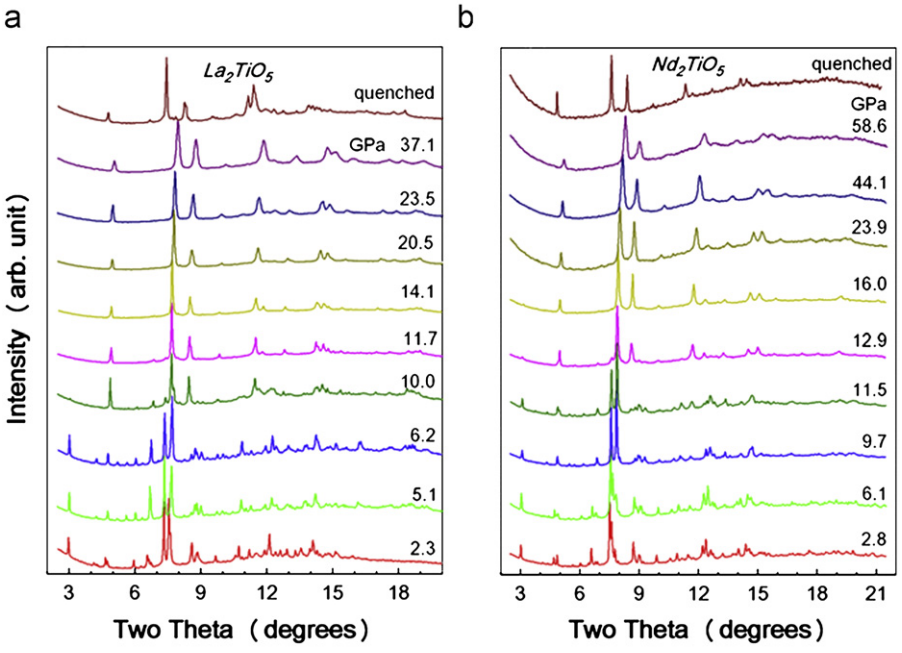

Fig. 3. Selected XRD patterns of (a) La_2TiO_5 and (b) Nd_2TiO_5 at different pressures (λ=0.4066 Å). A pressure-induced phase transition was obviously observed at 10.0 and 9.7 GPa in the two systems, respectively.

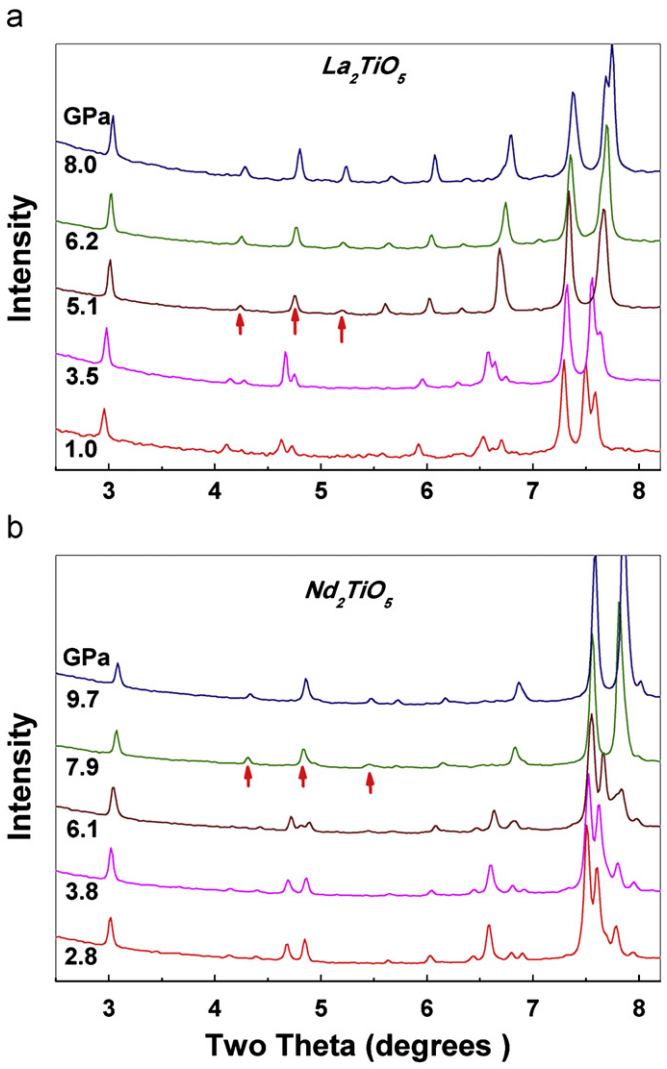

Fig. 4. Enlarged XRD patterns of (a) La_2TiO_5 and (b) Nd_2TiO_5 at pressures less than 10 GPa show that both compounds have a subtle structural change that is first evident at 5.1 and 6.1 GPa, respectively.

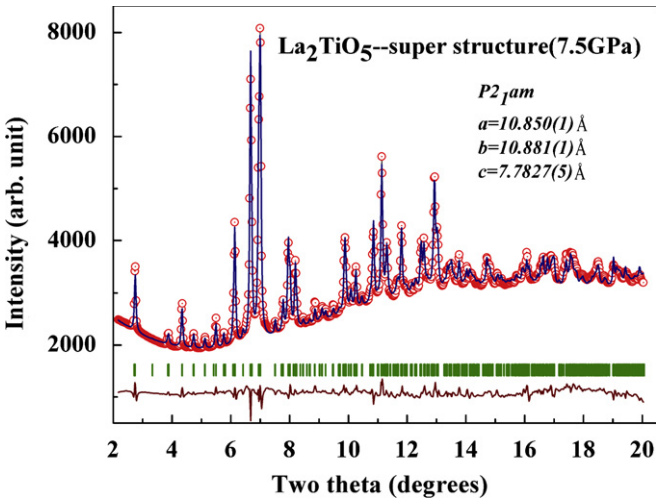

Fig. 5. XRD pattern of La_2TiO_5 at 7.5 GPa (λ=0.3681 Å) refined with an $a \times b \times 2c$ superstructure and space group of $P2_1am$, a, b, and c are the lattice parameters of the basic orthorhombic unit cell.

Table 2
Refinement results[a] of the superlattice of La_2TiO_5 at 7.5 GPa with space group of $P2_1am$ and lattice constants of a=10.8500(10) Å, b=10.8814(9) Å, c=7.7827(4) Å, resulting R_B=8.9% and χ^2=1.12.

Atom	Wyckoff	x/a	y/b	z/c
La1	2*a*	0.291(6)	0.329(2)	0
La2	2*b*	0.214(5)	−0.083(2)	1/2
La3	2*b*	0.294(6)	0.302(2)	1/2
La4	4*c*	0.533(5)	−0.183(2)	0.258(3)
La5	4*c*	0.572(5)	0.455(1)	0.258(3)
La6	2*a*	0.766(5)	0.025(2)	0
Ti1	4*c*	0.461(7)	0.101(3)	0.233(7)
Ti2	2*b*	0.855(7)	0.341(6)	1/2
Ti3	2*a*	0.342(8)	0.641(6)	0
O1	2*b*	0.4485	0.8510	1/2
O2	4*c*	0.5139	0.0246	0.9194
O3	2*b*	0.1910	0.5325	1/2
O4	2*a*	−0.0455	−0.1338	0
O5	2*b*	0.1754	0.1316	1/2
O6	4*c*	0.1823	0.3483	0.2185
O7	2*b*	0.4591	0.4842	1/2
O8	2*b*	0.5886	0.1166	1/2
O9	4*c*	0.4074	0.2884	0.2930
O10	4*c*	−0.1128	−0.0043	0.2963
O11	4*c*	0.3668	0.6342	0.7475
O12	2*a*	0.1970	0.5548	0
O13	2*a*	0.3929	0.7824	0
O14	2*a*	0.4595	0.4954	0
O15	2*a*	0.1608	0.1487	0

[a] Atoms O12–O15 were only determined by building proper five-coordinate TiO_5 polyhedra and the atomic coordinates of all O atoms are not refined.

light atoms are oxygen. In fact, the XRD pattern at high pressures is not good enough to generate all the oxygen positions in the unit cell using the fitting program. Since there is a close relation between the super cell and its basic unit cell, we believe that the local atomic bonding environment between the super cell and the basic cell should be quite similar. In the basic orthorhombic unit cell, Ti atoms are five-fold coordinated with oxygen. In comparison, we found that 4 additional oxygen atoms are required to build the superstructure model, which made a complete corner-shared TiO_5 polyhedra framework, and at the same time, resulted in an unchanged composition during the phase transition. The observed XRD pattern can be well refined with the proposed super cell structure model (Fig. 5). The refined lattice parameters and coordinates of all atoms are shown in Table 2. All of the positions of oxygen are not refined. The schematic crystal structure projected along the *c*-axis is shown in Fig. 6. By comparing Figs. 1 and 6, it is evident that the local atomic bonding environment of the superstructure is similar to that of the basic unit cell, and the main reason for the formation of super cell is that half of the lanthanide elements are rearranged in the *a*–*b* plane. In Fig. 6, some of the La atoms do not have the same *x*, *y* coordinates when viewed along the *c*-axis; thus, a larger *c*-axis is required in order to account for the periodicity along the *c*-axis.

Refinement of the lattice parameters before the second phase transition revealed the discontinuity of the lattice parameters during the formation of superstructure. The refined lattice parameters of La_2TiO_5 and Nd_2TiO_5 at lower pressures are shown in Fig. 7. Note for comparison that the *c*-axis of the super cell is shown as *c*/2. From Fig. 7, the discontinuous change of lattice parameters during the formation of superstructure is clearly evident. The *a* and *b* parameters show different trends during the phase transition; the *a* and *b* parameters are less different in the super cell. In fact, the super cell of La_2TiO_5 at 8 GPa is very close to a tetragonal unit cell. The refined data do not indicate any apparent volume change during the formation of the superstructure for La_2TiO_5, but there is a small amount of volume

shrinkage (~2.5%) in Nd_2TiO_5 system at 6.1 GPa. The pressure-induced formation of superstructure is a displacive process and half of the lanthanide elements are rearranged in the *a*–*b* plane.

3.2. Hexagonal high-pressure phase

As shown in Fig. 3, the high-pressure phase above 10 GPa has a simple XRD pattern, which suggests a higher symmetry. The indexed pattern confirmed that the high-pressure phase has a hexagonal unit cell, with a possible space group of $P6_3/mmc$. It has been reported [13] that some of the 215 phases, such as Gd_2TiO_5 and Y_2TiO_5 have a hexagonal ($P6_3/mmc$) polymorph. Based on the phase diagram, this is a high temperature phase, which is stable at temperatures above 1300 °C. However, the calculated XRD pattern of the hexagonal high temperature phase is very different from the observed XRD patterns of the high-pressure phase. The high-pressure and high temperature phases thus have different structures though they have the same symmetry. In order to identify the structure, we tried to solve the structure directly with software EXPO and also to find any isotropic structures in ICSD database. The results revealed that the high-pressure phase with space group of $P6_3/mmc$ may have a structure similar with

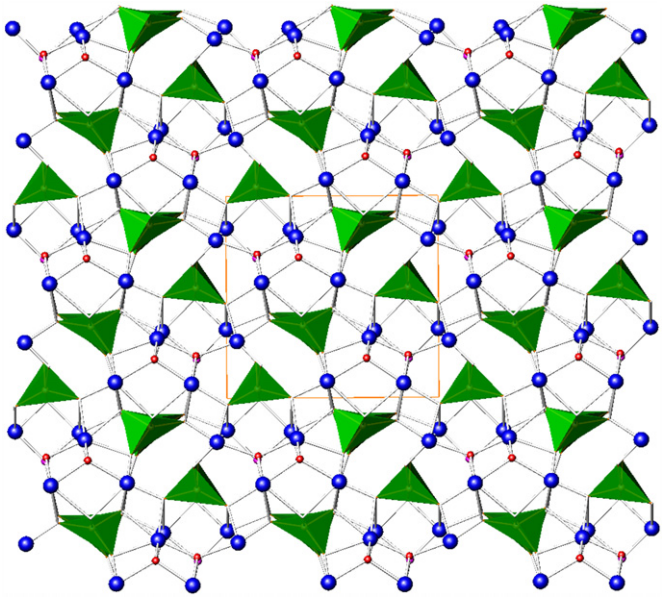

Fig. 6. Schematic crystal structure of the superstructure of Ln_2TiO_5 at high pressures projected along the *c*-axis.

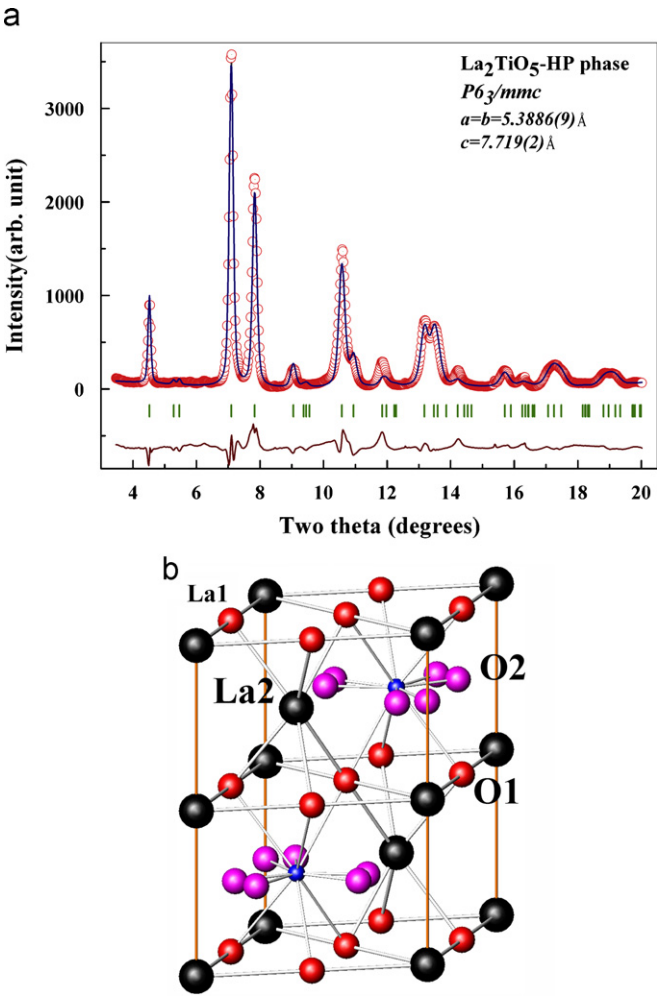

Fig. 8. The observed XRD patterns of the high-pressure phase was refined with a hexagonal structure model ($P6_3/mmc$): (a) XRD pattern of La_2TiO_5 at 20 GPa and its fitting results and (b) schematic crystal structure of the high-pressure phase.

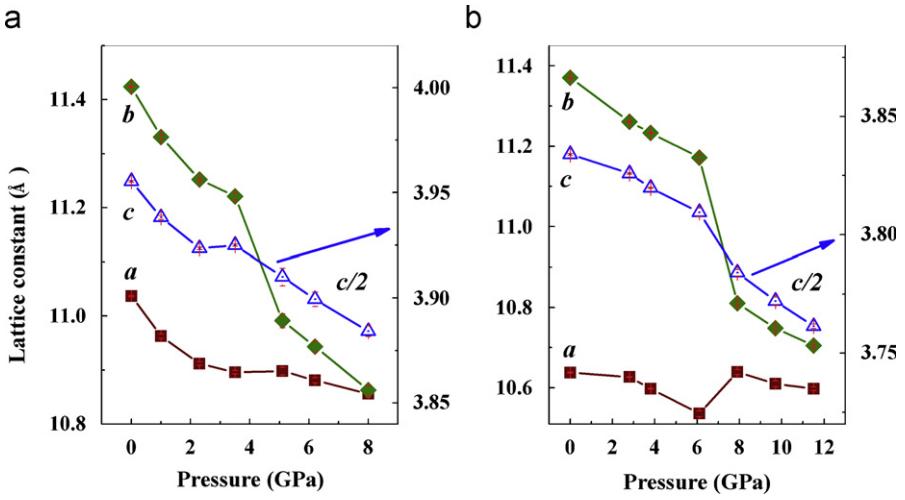

Fig. 7. Pressure dependence of the lattice constants of (a) La_2TiO_5 and (b) Nd_2TiO_5 before the second phase transition. There are obvious discontinuities between the *a* and *b* unit cell parameters during the phase transition. The superstructure of La_2TiO_5 is close to a tetragonal structure at 8 GPa.

Na_2SO_4. In the Na_2SO_4 structure, both of the two independent oxygen atoms in the unit cell occupy the 12*k* positions and have only a 1/3 occupancy rate. Based on the different sizes of the cations, we proposed a reasonable structure model, where the two oxygen atoms occupy the position of 6*g* and 12*j*, respectively. Fig. 8a shows the Rietveld refinement results of the XRD pattern of La_2TiO_5 measured at 20.9 GPa, and the details of the high-pressure phase are listed in Table 3. The schematic crystal structure is shown in Fig. 8b. Due to the splitting of the 12*j* position for oxygen, O_{12j} has a maximum occupancy of 0.5. In order to make a good fit, the 12*j* oxygen has an occupancy of only 0.21 based on the refinement. In addition, the first oxygen at 6*g* and second La position at 2*c* are also not fully occupied. Due to the partial occupancy, the oxygen atoms in the high-pressure phase are disordered. The bonding environment of Ti is different in the high-pressure phase, and the coordination number changes from 5 in the orthorhombic structure to more than 6 (due to the partial occupancies of O around it) in the hexagonal structure. From the crystal structure shown in Fig. 8b, it is clear that the pressure-induced phase transition from the orthorhombic to hexagonal structures is a reconstruction process, and the high-pressure phase is quenchable at ambient conditions (shown in Fig. 3). However, there are some weak diffraction peaks present in addition to those of the high-pressure phase in the quenched samples, especially evident in the pattern for La_2TiO_5. This is in agreement with the refinement results of the high-pressure phase. The partial occupancies of La_2 and O atoms in the hexagonal phase indicated that some decomposition occurred during the second pressure-induced phase transition, and the extra diffraction peaks in the quenched samples may be related to the decomposition products, e.g., LnO_x ($x=1$–2).

Based on the Rietveld refinement results, the pressure dependence of the unit cell volume for Nd_2TiO_5 is plotted in Fig. 9. The volume decreases 11% during the phase transition from the super cell to the hexagonal high-pressure phase at 11.5 GPa. There is also an obvious volume decrease for Nd_2TiO_5 during the formation of superlattice between 3.8 and 6.1 GPa. Fitting the PV curve with the Birch–Murnaghan equation of state yields a bulk modulus of 184(12) GPa, when the pressure derivative is fixed at 4. This value is comparable to the compressibility of $A_2B_2O_7$ pyrochlores in the same system. However, the starting orthorhombic phase is much easier to compress as compared with the pyrochlore structure. The estimated bulk modulus for the orthorhombic Nd_2TiO_5 is less than 100 GPa, but this does not consider the volume change during the formation of superlattice structure.

Table 3
Refinement results of the hexagonal high-pressure phase of La_2TiO_5 at 20.9 GPa with space group of $P6_3/mmc$ and lattice constants of $a=b=5.3886(9)$ Å, $c=7.718(2)$ Å, resulting $R_B=7.5\%$ and $\chi^2=6.9$.

Atom	Wyckoff	*x*/*a*	*y*/*b*	*z*/*c*	Occu.
La1	2*a*	0	0	1/2	1
La2	2*c*	2/3	1/3	3/4	0.53
Ti	2*d*	1/3	2/3	3/4	1
O1	6*g*	0	1/2	1/2	0.86
O2	12j	0.099	−0.672	3/4	0.21

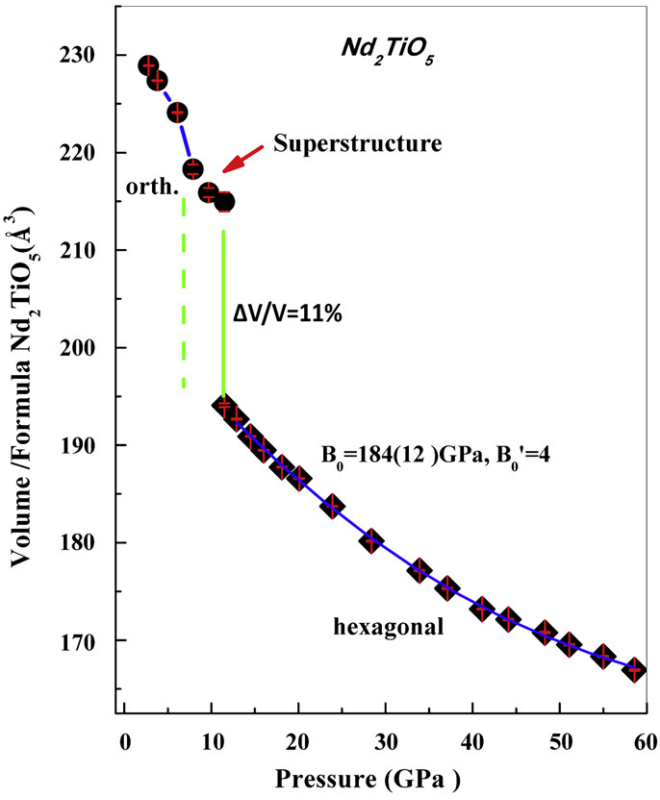

Fig. 9. *P*–*V* curve of Nd_2TiO_5. There is an obvious volume decrease (~2.5%) for Nd_2TiO_5 during the formation of superlattice, and the system has 11% volume reduction during the formation of the second high-pressure phase.

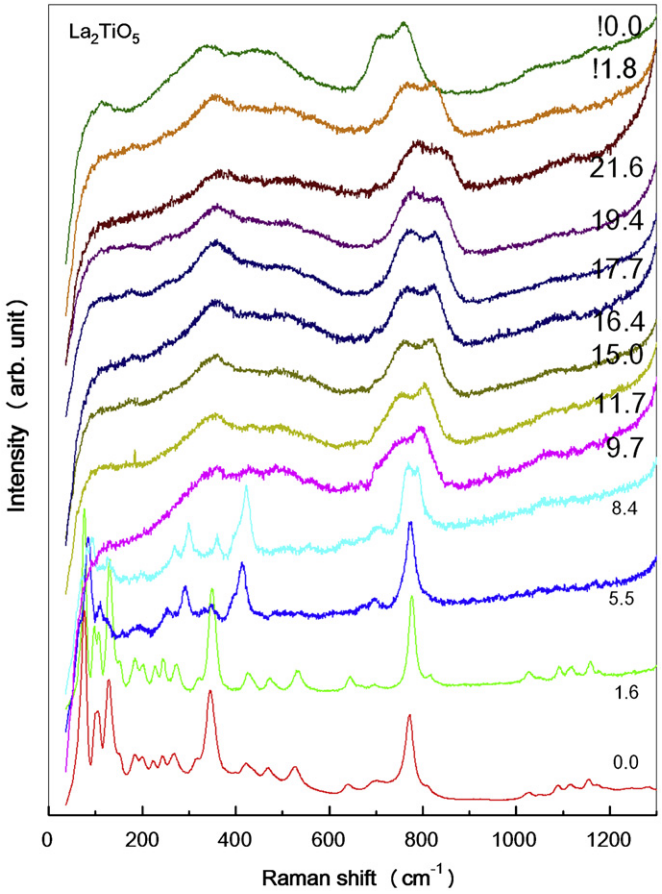

Fig. 10. Selected Raman spectra of La_2TiO_5 at various pressures. Two phase transitions were identified at 5.5 and 9.7 GPa, respectively, which is in good agreement with the observed XRD measurements. The second high-pressure phase is quenchable.

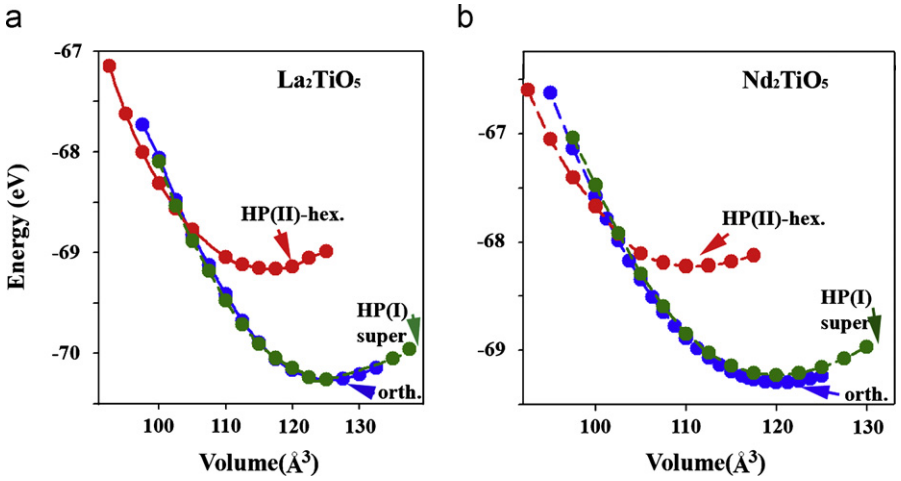

Fig. 11. Calculated *E–V* curves for (a) La_2TiO_5 and (b) Nd_2TiO_5 indicate that the orthorhombic phase is only stable at low pressures and transformed to the hexagonal phase at high pressures. The energy difference between the superlattice and its basic orthorhombic unit cell is very small.

3.3. Raman measurements

The powder samples were also investigated by Raman spectroscopy. Selected Raman spectra for La_2TiO_5 at different pressures are shown in Fig. 10. Due to the large lattice parameters and low symmetry of the unit cell, the starting orthorhombic phase has a quite complicated Raman spectrum, and more than 20 Raman active modes are clearly observed. There is no previous report on the Raman spectrum of any 215 phases, however, based on the atomic masses, we can conclude that the modes below 200 cm^{-1} are mainly due to the heavy lanthanide elements, and the strong band at frequency around 770 cm^{-1} is contributed to the Ti–O bonds in the TiO_5 polyhedron. At 5.5 GPa, a new Raman mode appeared at 400 cm^{-1}, but the main character of the spectrum remains the same. This was caused by the formation of superlattice, which is consistent with the XRD results. At higher pressures, the Raman modes became weak, and most of the sharp modes disappeared, and only the strong bands due to the TiO_5 polyhedra remained. The Raman signal clearly indicated that a phase transition occurred at 9.7 GPa in La_2TiO_5. There are only two main bands observed in the high-pressure phase, and they have frequencies at 200–600 and 700–800 cm^{-1}, respectively. The Raman band between 700 and 800 cm^{-1} for the high-pressure phase is obviously different from the band at low pressures. Although the peaks broaden at high pressures, it is clear that the band splits and contains more than one Raman active mode, which suggests that the TiO_5 polyhedra have been changed in the high-pressure phase. The Raman spectra of the quenched sample also revealed that the high-pressure phase is quenchable.

3.4. Theoretical calculations

A quantum mechanical calculation was made based on the three structural models in La_2TiO_5 and Nd_2TiO_5 systems. The calculated enthalpy volume curves are plotted in Fig. 11. The orthorhombic superlattice has a structure closely related to the basic orthorhombic unit cell, so there is little difference in the bulk energies. The partial occupancy of atoms in the hexagonal phase was not considered during calculation, and the results indicated that the hexagonal phase is a high-pressure structure and only stable at high pressures. The transition pressure derived from the calculated energy curve is in good agreement with observed values. Thus, the calculations are in good agreement with the experimental results.

4. Summary

Orthorhombic La_2TiO_5 and Nd_2TiO_5 were studied at high pressure by XRD, Raman scattering measurements and quantum mechanical calculations. Two new structures, which were induced by high pressure, were identified. At pressures between 5 and 10 GPa, an orthorhombic super cell ($a \times b \times 2c$) was formed, which is due to the rearrangement of the lanthanide cations in the *a–b* plane. With a further increase of pressure, a reconstructive phase transition occurred. The second high-pressure phase is hexagonal with a decrease of 11% in volume based on the XRD analysis. With the second phase transition, a small amount of lanthanide oxide forms as a decomposition product of the 215 phase, and the second high-pressure phase is quenchable. The two pressure-induced phase transitions in these 215 phases were verified by Raman scattering measurement, and the relative energetics of the phases made with quantum mechanical calculations, which accurately predicted the pressures of the phase transitions.

Acknowledgments

This work was supported by the Office of Basic Energy Sciences of the US Department of Energy, through Grant no. DE-FG02-97ER45656. The use of the beam line at X17C station of NSLS is supported by NSF COMPRES EAR01-35554 and by US-DOE contract DE-AC02-10886. The synchrotron experiments performed at HPCAT (Sector 16), Advanced Photon Source (APS), Argonne National Laboratory is supported by DOE-BES, DOE-NNSA, NSF, and the W.M. Keck Foundation. APS is supported by DOE-BES, under Contract no. DE-AC02-06CH11357.

References

[1] H. Tanaka, J. Zhang, T. Kawai, Phys. Rev. Lett. 88 (2002) 027204.
[2] D.A. Muller, N. Nakagawa, A. Ohtomo, J.L. Grazul, H.Y. Hwang, Nature 430 (2004) 657.
[3] G.C. Lau, R.S. Freitas, B.G. Ueland, B.D. Muegge, E.L. Duncan, P. Schiffer, R.J. Cava, Nat. Phys. 2 (2006) 249.
[4] Y. Machida, S. Nakatsuji, S. Onoda, T. Tayama, T. Sakakibara, Nature 463 (2010) 210.
[5] K. Page, T. Kolodiazhnyi, T. Proffen, A.K. Cheetham, R. Seshadri, Phys. Rev. Lett. 101 (2008) 205502.
[6] S.T. Bramwell, M.J.P. Gingras, Science 294 (2001) 1495.
[7] I. Mirebeau, I.N. Goncharenko, P. Cadavez-Pares, S.T. Bramwell, M.J.P. Gingras, J.S. Gardner, Nature 420 (2002) 54.

[8] G.C. Lau, T.M. McQueen, Q. Huang, H.W. Zandergen, R.J. Cava, J. Solid State Chem. 181 (2008) 45.
[9] G.C. Lau, R.S. Freitas, B.G. Ueland, M.L. Dahlberg, Q. Huang, H.W. Zandbergen, P. Schiffer, R.J. Cava, Phys. Rev. B 76 (2007) 054430.
[10] J.P.C. Ruff, B.D. Gaulin, J.P. Castellan, K.C. Rule, J.P. Clancy, J. Rodriguez, H.A. Dabkowska, Phys. Rev. Lett. 99 (2007) 237202.
[11] F. Lichtenberg, A. Herrnberger, K. Wiedenmann, J. Mannhart, Prog. Solid State Chem. 29 (2001) 1.
[12] W.G. Mumme, A.D. Wadsley, Acta Crystallogr. B24 (1968) 1327.
[13] Yu.F. Shepelev, M.A. Petrova, Inorg. Mater. 44 (2008) 1354.
[14] M.A. Petrova, A.S. Novikova, R.G. Grebenshchikov, Inorg. Mater. 39 (2003) 509.
[15] S.D. Skapin, D. Kolar, D. Suvorov, J. Eur. Ceram. Soc. 20 (2000) 1179.
[16] N. Jaouen, A.C. Dhaussy, J.P. Itie, A. Rogalev, S. Marinel, Y. Joly, Phys. Rev. B 75 (2007) 224115.
[17] J. Rouquette, J. Haines, V. Bornand, M. Pintard, P. Papet, R. Astier, J.M. Leger, F. Gorelli, Phys. Rev. B 65 (2002) 214102.
[18] M. Fischer, B. Bonello, J.P. Itie, A. Polian, E. Dartyge, A. Fontaine, H. Tolentino, Phys. Rev. B 42 (1990) 8494.
[19] F.X. Zhang, J. Lian, U. Becker, R.C. Ewing, L.M. Wang, J. Hu, S.K. Saxena, J. Solid State Chem. 180 (2007) 571–576.
[20] E. Bousquet, P. Ghosez, Phys. Rev. B 74 (2006) 180101.
[21] F.X. Zhang, B. Manoun, S.K. Saxena, C.S. Zha, Appl. Phys. Lett. 86 (2005) 181906.
[22] F.X. Zhang, J.W. Wang, J. Lian, M.K. Lang, U. Becker, R.C. Ewing, Phys. Rev. Lett. 100 (2008) 045503.
[23] F.X. Zhang, J. Lian, J.M. Zhang, K.J. Moreno, A.F. Fuentes, Z.W. Wang, R.C. Ewing, J. Alloys Compd. 494 (2010) 34.
[24] A.P. Hammersley, Fit 2d, ESRF, Grenoble, France, 1998.
[25] J. Rodriguez-Carvajal, Fullprof 2k, France, 2001.
[26] A. Boultif, D. Louer, J. Appl. Crystallogr. 37 (2004) 724.
[27] A. Altomare, R. Caliandro, M. Camalli, C. Cuocci, I. da Silva, C. Giacovazzo, A.G.G. Moliterni, R. Spagna, J. Appl. Crystallogr. 37 (2004) 957.
[28] J. Hafner, Comput. Phys. Commun. 177 (2007) 6.
[29] P.E. Blöchl, Phys. Rev. B 50 (1994) 17953.
[30] J.P. Perdew, et al., Phys. Rev. B 46 (1992) 6671.
[31] J.P. Perdew, Y. Wang, Phys. Rev. B 45 (1992) 13244.
[32] J.P. Perdew, Y. Wang, Phys. Rev. B 33 (1986) 8800.